# Influence of $Xe_2^+$ ions on the micro-hollow cathode discharge driven by thermionic emission

D. Levko,[1] Y. P. Bliokh,[2] and Ya. E. Krasik[2]
[1]*LAPLACE (Laboratoire Plasma et Conversion d'Energie), Universite de Toulouse, UPS, INPT Toulouse, 118 Route de Narbonne, F-31062 Toulouse Cedex 9, France*
[2]*Department of Physics, Technion, 32000 Haifa, Israel*

(Received 24 March 2014; accepted 31 March 2014; published online 16 April 2014)

The influence of $Xe_2^+$ dimer ions and excited Xe* atoms on the hollow cathode discharge driven by electron thermionic emission is studied using two-dimensional Particle-in-Cell Monte Carlo Collisions modeling. A comparison with the results of two-component (electrons and $Xe^+$ ions) plasma modeling showed that the presence of the $Xe_2^+$ dimer ions and excited Xe* atoms in the plasma affects the plasma parameters (density, potential, and ion fluxes toward the cathode). The influence of $Xe_2^+$ ions and Xe* atoms on the plasma sheath parameters, such as thickness and the ion velocity at the sheath edge, is analyzed. © *2014 AIP Publishing LLC*. [http://dx.doi.org/10.1063/1.4871487]

## I. INTRODUCTION

Today, the discharges of hollow cathodes (HCs), which operate with significantly larger current densities than do planar diodes, are widely used in many applications, such as spectral lamps,[1] lasers,[2] surface modification,[3] and electric propulsion.[4–9] Depending on the technological application, HC high current discharge is ignited and sustained by different electron emission mechanisms, namely, field, secondary, photo, or thermionic emission, or a combination of these electron emission mechanisms. The HCs driven by thermionic emission are used in applications related to electric propulsion;[4–9] we will consider only this type of HC below.

In a recent paper,[9] we reviewed the Particle-in-Cell (PIC), fluid, and hybrid models used by different groups for analyzing thermionic emission HC operation. It is important to note that these models consider three plasma species (electron, ion, and neutral), and excited atoms or multi-charged ion species were not taken into account. The latter were considered in the fluid models of the HC discharge used in spectral lamps and laser applications (see, e.g., Refs. 2 and 10). For instance, an important role of metastable atoms in the operating conditions of HCs is reported in Ref. 10. Therefore, one can suppose that such particles could play an important role in thermionic HCs as well.

In recent studies in the literature (see Refs. 11–13 and references therein), the ion Bohm velocity in plasma consisting of two and more ion species is still discussed and investigated using different methods. Knowledge about this ion velocity is very important in fluid models, since it determines the boundary conditions. Baalrud *et al.*[13] showed that in multicomponent plasma, depending on the ratios between different ion masses and densities, two different scenarios can be realized. Namely, for some conditions, two-stream instability is excited in the plasma pre-sheath and different ions entering the sheath have the same velocity. Otherwise, each plasma species enters the sheath with its individual ion sound velocity.

Unlike in fluid models, the addition of the second ion specie in the Particle-in-Cell model does not require different regimes that are modeled self-consistently (see, e.g., Ref. 13). In the present paper, the influence of excited Xe* atoms and ionized dimer $Xe_2^+$ on the HC discharge driven by thermionic emission is studied. The two-dimensional PIC Monte Carlo Collision model (2D PIC/MCC) is used for the self-consistent modeling of this type of discharge, with special attention being paid to the influence of $Xe_2^+$ dimer ions on the plasma sheath parameters.

## II. NUMERICAL MODEL

The 2D PIC/MCC model was described in detail in our recent paper.[9] This model is based on the 2D Cartesian module of the open-source WARP[14] PIC code. In order to study the influence of ionized dimers $Xe_2^+$ on the micro-hollow cathode discharge in the geometry shown in Fig. 1, two models of the plasma are considered. In the first model, the plasma consists of only electrons and ions $Xe^+$ (hereafter, two-component plasma). In the second model, the plasma contains also $Xe_2^+$ dimer ions and excited Xe* atoms (hereafter, many-component plasmas). A set of reactions (see Table I) in which $Xe_2^+$ ions and Xe* atoms participate is incorporated into the model.

The collisions that involve Xe atoms (see reactions #7–11 in Table I) are modeled using the rate constant $k_i$ of the corresponding reaction, described in Refs. 15 and 16. Namely, after a fixed number of time steps, $N_{dt}$, the number of particles that experienced each type of collision is defined as $N_{C,i} = N_{Xe^*} \cdot k_i \cdot n_p \cdot N_{dt} \cdot dt$, where $N_{Xe^*}$ is the number of Xe* atoms presented in the simulation domain and $n_p$ is the density of the colliding partner. Then, the number $N_{C,i}$ of Xe* particles is chosen randomly and, depending on the type of collision, different conditions are applied to these particles. If reaction #7 occurs, only the direction of Xe* propagation is changed. The angles after collision are calculated using the equations described in Ref. 9. If reaction #8 occurs, the excited atom is removed from the simulations and the colliding electron obtains an additional energy that is equal to the energy of Xe atom excitation. If reaction #9 or #10 occurs, two excited atoms are removed from the simulations, and ions $Xe^+$ or $Xe_2^+$ and an electron are added. Both

 

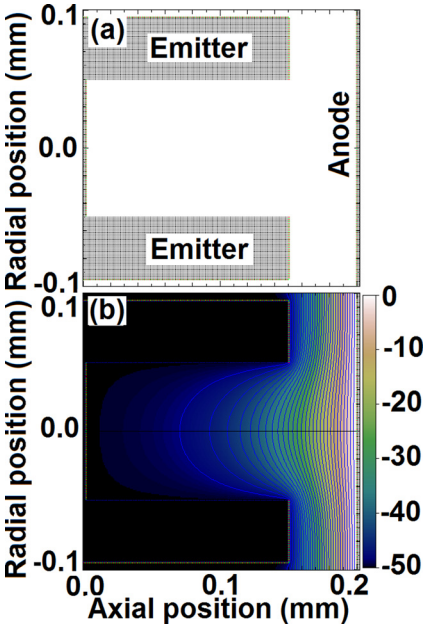


FIG. 1. (a) Geometry of the micro-hollow cathode considered in the 2D PIC/MCC model and (b) two-dimensional potential profile at $t = 0$.

particles have energy equal to the energy of Xe atom excitation. If reaction #11 occurs, the excited atom is removed and the energies of colliding and generated electrons are calculated as for reaction #1 with a corresponding ionization threshold.

Each computational cycle with time step $dt$ consists of the following steps:

1. Electron emission from the surface of the HC emitter is described by the Richardson-Dushman[4] law that accounts for the Schottky effect

$$J(x) = DT^2 \exp\left(\frac{-e\varphi_0}{kT}\right) \cdot \exp\left(\frac{e}{kT}\sqrt{\frac{eE_C(x)}{4\pi\varepsilon_0}}\right). \quad (1)$$

Here, $e$ is an elementary charge, $E_C(x)$ is the electric field at the cathode surface, $D = 1.1 \times 10^6\,\mathrm{A\cdot m^{-2}\,K^{-2}}$ is the constant, whose value is defined by the emitter material,[4] $T$ is the temperature of the emitter, and $\varphi_0$ is the emitter work function. In the model, the value $\varphi_0 \approx 1.8\,\mathrm{eV}$ (see Ref. 4) and the temperature of the emitter $T = 1300\,\mathrm{K}$ are used.
2. Calculation of the self-consistent electric field; determination of new velocities and positions of the particles using equations of motion.
3. Determination of number and total energy of ions reaching the emitter surface (these ions cause the secondary electron emission (SEE)).
4. Removal of the particles reaching the cathode and anode surfaces and boundaries of the simulation region.
5. Calculation of the electron-neutral, neutral-neutral, electron-ion and ion-neutral collisions.
6. Calculation of the secondary electron emission.
7. Return to the step #1.

TABLE I. Set of collision reactions considered in 2D PIC/MCC model.

| | Reaction | Type | References |
|---|---|---|---|
| 1 | $Xe + e \rightarrow Xe^+ + 2e$ | Ionization | 9 |
| 2 | $Xe + e \rightarrow Xe + e$ | Elastic | 9 |
| 3 | $Xe + e \rightarrow Xe^* + e$ | Excitation | 9 |
| 4 | $Xe^+ + e \rightarrow Xe^+ + e$ | Coulomb | 9 |
| 5 | $Xe^+ + Xe \rightarrow Xe + Xe^+$ | Charge exchange | 9 |
| 6 | $Xe^+ + Xe \rightarrow Xe^+ + Xe$ | Elastic | 9 |
| 7 | $Xe^* + Xe \rightarrow Xe^* + Xe$ | Elastic | 15 |
| 8 | $Xe^* + e \rightarrow Xe + e$ | De-excitation | 15 |
| 9 | $Xe^* + Xe^* \rightarrow Xe + Xe^+ + e$ | Ionization | 15 |
| 10 | $Xe^* + Xe^* \rightarrow Xe_2^+ + e$ | Ionization | 16 |
| 11 | $Xe^* + e \rightarrow Xe^+ + 2e$ | Ionization | 15 |
| 12 | $Xe_2^+ + Xe \rightarrow Xe_2^+ + Xe$ | Elastic | 15 |

## III. RESULTS AND DISCUSSION

The 2D PIC/MCC modeling was carried out for a HC having an inner diameter of 0.1 mm, outer diameter of 0.19 mm, and length of 0.15 mm. The distance between the HC and anode is 0.05 mm. The neutral gas pressure is $10^3$ Pa and the HC voltage is $\varphi_C = -50$ V; the anode is grounded. In the model, neutrals are considered as a background having uniform density. The temperature of the neutral gas is assumed equal to the HC temperature of 1300 K. The masses of $Xe^+$ and $Xe_2^+$ particles are taken equal to 1 amu and 2 amu, respectively.

The simulations show that the HC develops as in the case studied in Ref. 9. The 2D plots of steady-state potential distribution and plasma species densities are presented in Fig. 2. One can see the generation of high-density plasma ($n_e \sim 10^{20}\,\mathrm{m^{-3}}$), which penetrates inside the HC and changes drastically the initial distribution of potential (see Fig. 1(b)).

A comparison of the profiles of the plasma species densities in two- and many-component plasmas models is shown in Fig. 3. One can see that the plasma density in many-component plasmas exceeds that in two-component plasma. This is due to three additional channels leading to the plasma generation (reactions #9, #10, and #11 in Table I). The

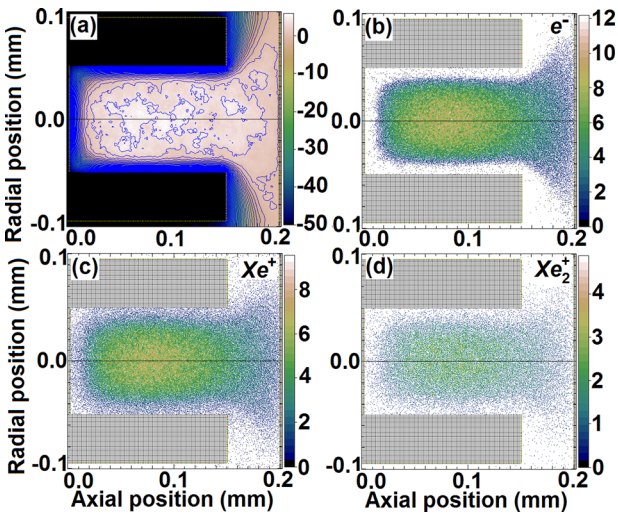


FIG. 2. Steady-state distributions of potential (a), electron density (b), density of $Xe^+$ ions (c), and density of ionized dimmers $Xe_2^+$. Plasma species densities should be multiplied by the factor of $10^{20}\,\mathrm{m^{-3}}$.

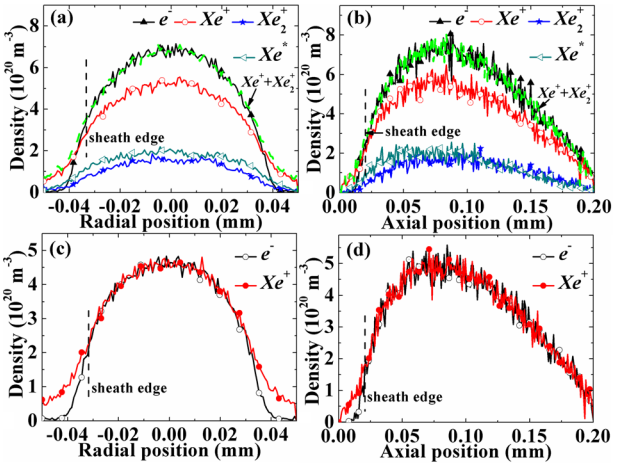


FIG. 3. Density of plasma species in (a) radial direction and (b) axial direction in many-component plasmas; density of plasma species in (c) radial direction and (d) axial direction in two-component plasma.

excitation cross section of Xe atoms is smaller than those of ionization (reaction #1). Therefore, the density of Xe* is smaller than that of $Xe^+$ ions. Let us note that, due to the fact that the excitation energy of Xe atoms (8.4 eV) is smaller than the ionization energy (12.1 eV), the ionization energy of Xe* atoms is only 3.7 eV.

Table II shows the contribution of different reactions to electron plasma density $n_e$. One can see that reaction #10, contributing to the build-up of $n_e$, is the collision between two excited Xe* atoms, which also results in the generation of $Xe_2^+$ ions. In addition, one can see that the contribution of this reaction is two times larger than the contribution of the similar channel leading to the generation of $Xe^+$ ions. The latter is explained by the large rate constant ($10^{-15}$ m$^3$ s$^{-1}$) of reaction #10, which is two times larger than those of reaction #9 ($0.5 \times 10^{-15}$ m$^3$ s$^{-1}$).

Figs. 3(a) and 3(b) show that the density of ionized dimmers $Xe_2^+$ is smaller than that of $Xe^+$ ions and is comparable with the density of excited Xe* atoms. This can be explained by the generation of $Xe_2^+$ ions by the collisions between two excited Xe* atoms (reaction #10). This process also explains the comparable densities of $Xe_2^+$ ions and Xe* atoms.

A comparison between radial (in the middle of the HC) and axial (at $y = 0$) distributions of the potential is shown in Fig. 4. One can see that the plasma potential slightly increases in the many-component plasmas as compared with the two-component plasma. The sheath edge location does not depend noticeably on the plasma (Figs. 3 and 4). Here, the sheath edge is defined as the position where the plasma quasineutrality is violated. This can be understood from the expression[17] for sheath thickness, $s \approx (\sqrt{2}/3)\lambda_{Ds}(2e|\phi_C|/kT_e)^{3/4}$, where $\lambda_{Ds}$ is the Debye length at the sheath edge. Here, an approximate equality is used because it does not take into account the

TABLE II. Contribution of different reactions to the electron density.

| R. 1 | R. 9 | R. 10 | R. 11 |
|---|---|---|---|
| 72% | 9% | 18% | 1% |

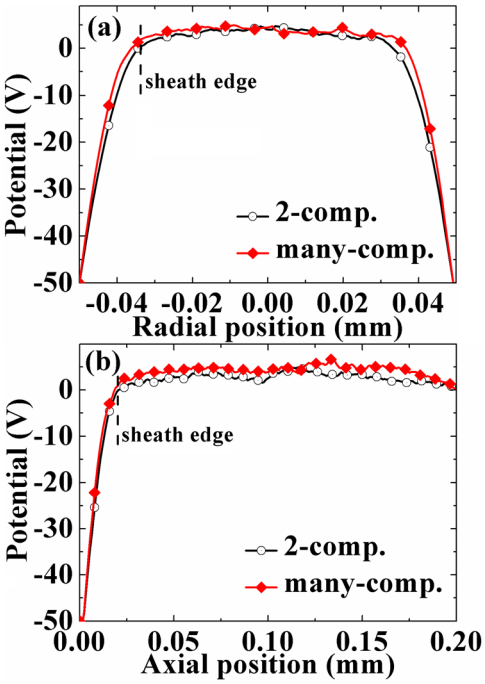


FIG. 4. Comparison of profiles of potential in (a) the radial and (b) the axial direction obtained for two- and many-component plasmas.

voltage between the cathode and sheath edge, but uses only cathode potential. Simulation results show that $T_{e1} \approx 2.0$ eV and $n_{es,1} \approx 2.4 \times 10^{20}$ m$^{-3}$ for two-component plasma, and $T_{e2} \approx 1.6$ eV and $n_{es,2} \approx 3.5 \times 10^{20}$ m$^{-3}$ for many-component plasmas. Taking into account that $\lambda_{Ds} \propto (T_e/n_{es})^{1/2}$, one can conclude that the ratio between the sheath thicknesses in the two plasmas is $s_1/s_2 = (T_{e2}/T_{e1})^{1/4}(n_{es,2}/n_{es,1})^{1/2} \approx 1.14$.

An increase in the plasma density leads to an increase in the ion flux to the cathode and, respectively, to an increase in

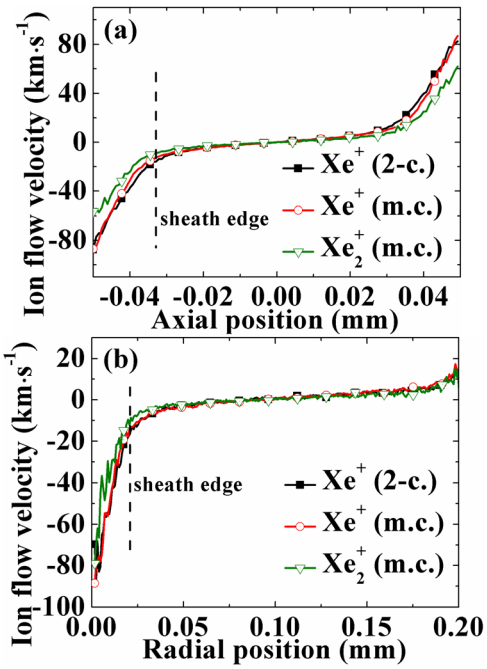


FIG. 5. Comparison of ion flow velocity in (a) the radial and (b) the axial direction obtained for two- and many-component plasmas.

TABLE III. Ion velocity at the sheath edge obtained in 2D PIC/MCC model and $c_{s,i} = \sqrt{kT_e/M_i}$.

| | Two-component | | | Many-component | | | | |
|---|---|---|---|---|---|---|---|---|
| | | | | $V_i$ 2D PIC/MCC (km·s$^{-1}$) | | | $c_{s,i}$ (km·s$^{-1}$) | |
| | $V_i$ 2D PIC/MCC (km·s$^{-1}$) | $T_e$ (eV) | $c_{s,i}$ (km·s$^{-1}$) | $Xe^+$ | $Xe_2^+$ | $T_e$ (eV) | $Xe^+$ | $Xe_2^+$ |
| Axial | 13.97 | 2.0 | 13.85 | 12.55 | 8.75 | 1.6 | 12.4 | 8.76 |
| Radial | 16.0 | 2.7 | 16.1 | 13.9 | 10.4 | 2.1 | 14.1 | 10.0 |

the ion energy delivered to the cathode. The latter will lead to an increase in the HC sputtering and, respectively, it will decrease the HC lifetime. Indeed, in the case of multi-component plasma, the results of simulations show that the current densities of $Xe^+$ and $Xe_2^+$ ions averaged along the cathode surface are 12 MA·m$^{-2}$ and 2 MA·m$^{-2}$, respectively, as compared with 9 MA·m$^{-2}$ ion current density in the case of two-component plasma.

As shown in Ref. 18, the Bohm criterion for plasma consisting of two different types of positive ions having densities $n_1$ and $n_2$, reads as

$$\frac{n_1}{n_e}\frac{c_{s1}^2}{V_1^2} + \frac{n_2}{n_e}\frac{c_{s2}^2}{V_2^2} \le 1. \quad (2)$$

Here, $V_1$ and $V_2$ are the ion velocities at the sheath edge and $c_{s,i} = \sqrt{kT_e/M_i}$ is the sound velocity of specie $i$. The present simulations show that at the sheath edge the ions have almost the same energies equal to $kT_e$. As a consequence, one can conclude from Eq. (2) that each ion specie leaving the sheath edge has its individual sound velocity $V_i = \sqrt{kT_e/M_i}$. This is confirmed by the results of simulations presented in Fig. 5 and in Table III. One can see that $Xe_2^+$ ions have a smaller velocity at the sheath edge. The results of the modeling of multi-component plasma showed also that $n_1/n_e \approx 0.85$ and $T_e/T_i \approx 4$, where $n_1$ and $T_i$ are the density and temperature of $Xe^+$, respectively. Following Ref. 13, these parameters are insignificant for the occurrence of two-stream instabilities in the pre-sheath and, therefore, our model shows that $V_1 \neq V_2$.

Finally, the results of 2D PIC/MCC simulations show an insignificant influence of thermionic emitted electrons on the Bohm velocity. This effect was discussed, for instance, in Ref. 19. Simulation results show that the sheath potential is about of 1 V and the ratio between thermionic current and discharge current is $\sim 10^{-3}$. For these parameters, the model studied in Ref. 19, see Eq. (10), predicts a $\sim$1% deviation of ion velocities at the sheath edge from the classical Bohm criterion. A comparison of the ion velocities $V_i$ at the sheath edge, obtained in modeling and calculated following the Bohm criterion as $c_{s,i} = \sqrt{kT_e/M_i}$, is presented in Table III. One can see that the difference between $V_i$ and $c_{s,i}$ is about $\sim$1%, which agrees well with the results presented in Ref. 19.

## IV. SUMMARY

Two-dimensional Particle-in-Cell Monte Carlo Collision modeling of the HC discharge driven by electron thermionic emission has been conducted. Two types of plasmas were studied: plasma consisting of electrons and $Xe^+$ ions, and plasma consisting of electrons and $Xe^+$ and $Xe_2^+$ ions and excited Xe* atoms. It was shown that the presence of the second ion specie increases the plasma density. This results in an increase in the energy of ions bombarding the cathode surface and increases the total ion current to the cathode, which must lead to a decrease in the cathode lifetime.

Comparison of the velocities of $Xe^+$ and $Xe_2^+$ ions at the sheath edge shows that each kind of ions enters the sheath with its individual sound speed. This allows one to conclude that the two-stream instability is not excited in the pre-sheath under the given conditions. In addition, numerical modeling showed the insignificant influence of the thermo-emitted electron beam current on the ion velocity at the sheath edge. For the considered conditions, this velocity can be defined by the classical Bohm criterion.

[1]J. V. Sullivan and A. Walsh, Spectrochim. Acta **21**, 721 (1965).
[2]D. Mihailova, J. van Dijk, G. J. M. Hagelaar, S. Karatodorov, P. Zahariev, M. Grozeva, and J. J. A. M. van der Mullen, J. Phys. D: Appl. Phys. **45**, 165201 (2012).
[3]J. Hopwood, *Ionized Physical Vapor Deposition*, Thin Film Series Vol. 27 (Academic Press, San Diego, 2000).
[4]D. Goebel and I. Katz, *Fundamentals of Electric Propulsion* (John Wiley & Sons, 2008).
[5]E. Oks, *Plasma Cathode Electron Sources* (Wiley-VCH, 2006).
[6]G. J. Kim, F. Iza, and J. K. Lee, J. Phys. D: Appl. Phys. **39**, 4386 (2006).
[7]V. Vekselman, Ya. E. Krasik, S. Gleizer, V. Tz. Gurovich, A. Warshavsky, and L. Rabinovich, J. Propul. Power **29**, 475 (2013).
[8]I. G. Mikellides, D. M. Goebel, J. S. Snyder, I. Katz, and D. A. Herman, J. Appl. Phys. **108**, 113308 (2010).
[9]D. Levko, Ya. E. Krasik, V. Vekselman, and I. Haber, Phys. Plasmas **20**, 083512 (2013).
[10]S. He, H. Jing, S. Liu, and J. Ouyang, Phys. Plasmas **20**, 123504 (2013).
[11]S. D. Baalrud and C. C. Hegna, Phys. Plasmas **18**, 023505 (2011).
[12]J. T. Gudmundsson and M. A. Lieberman, Phys. Rev. Lett. **107**, 045002 (2011).
[13]S. D. Baalrud, T. Lafleur, W. Fox, and K. Germaschewski, "Instability-enhanced friction in the pre-sheath of two-ion-species plasmas," available at http://newton.physics.uiowa.edu/~sbaalrud/publications.html (submitted).
[14]D. P. Grote, A. Friedman, J. L. Vay, and I. Haber, AIP Conf. Proc. **749**, 55 (2005).
[15]L. A. Levin, S. E. Moody, E. L. Klosterman, R. Center, and J. Ewing, IEEE J. Quantum Electron. **17**, 2282 (1981).
[16]F. Kannari, A. Suda, M. Obara, and T. Fujioka, IEEE J. Quantum Electron. **19**, 1587 (1983).
[17]M. A. Lieberman and A. J. Lichtenberg, *Principles of Plasma Discharges and Materials Processing* (Wiley-Intersciences, New York, 2005).
[18]K.-U. Riemann, IEEE Trans. Plasma Sci. **23**, 709 (1995).
[19]J. H. Palacio Mizrahi and Ya. E. Krasik, Phys. Plasmas **20**, 083510 (2013).